Soil and ribbed concrete slab interface modeling using large shear box and 3D FEM

Article · February 2017

DOI: 10.12989/gae.2017.12.2.295

5 authors, including:

Jiangu Qian
Tongji University
79 PUBLICATIONS **323** CITATIONS

SEE PROFILE

Geomechanics and Engineering, *Vol. 12*, *No. 2* (*2017*) *295-312*
DOI: https://doi.org/10.12989/gae.2017.12.2.295

Soil and ribbed concrete slab interface modeling using large shear box and 3D FEM

Jian-Gu Qian [*1], Qian Gao [1], Jian-feng Xue [2], Hong-Wei Chen [3] and Mao-Song Huang [1]

[1] *Department of Geotechnical Engineering, Tongji University, Shanghai, 200092, China*
[2] *School of Engineering and IT, Federation University, Churchill, 3842, VIC, Australia*
[3] *Department of Underground Structure & Geotechnical Engineering, East China Architecture Design & Research Institute Co., Ltd., Shanghai 200002, China*

(*Received December 16, 2015, Revised October 03, 2016, Accepted October 25, 2016*)

Abstract. Cast in situ and grouted concrete helical piles with 150-200 mm diameter half cylindrical ribs have become an economical and effective choice in Shanghai, China for uplift piles in deep soft soils. Though this type of pile has been successful used in practice, the reinforcing mechanism and the contribution of the ribs to the total resistance is not clear, and there is no clear guideline for the design of such piles. To study the inclusion of ribs to the contribution of shear resistance, the shear behaviour between silty sand and concrete slabs with parallel ribs at different spacing and angles were tested in a large direct shear box (600 mm × 400 mm × 200 mm). The front panels of the shear box are detachable to observe the soil deformation after the test. The tests were modelled with three-dimensional finite element method in ABAQUS. It was found that, passive zones can be developed ahead of the ribs to form undulated failure surfaces. The shear resistance and failure mode are affected by the ratio of rib spacing to rib diameter. Based on the shape and continuity of the failure zones at the interface, the failure modes at the interface can be classified as "punching", "local" or "general" shear failure respectively. With the inclusion of the ribs, the pull out resistance can increase up to 17%. The optimum rib spacing to rib diameter ratio was found to be around 7 based on the observed experimental results and the numerical modelling.

Keywords: soil and ribbed concrete interface resistance; cast in-situ concrete helical piles; optimum rib spacing; undulated shear failure surface

1. Introduction

Most part of Shanghai, China is covered with thick layer of soft soils, e.g., 30 meters or thicker. Helical piles are often used to resist uplift loading. To accommodate the thick layer of soft soils, Qian *et al*. (2013) reported a new type of cast in-situ grouted helical pile by inclusion of cylindrical ribs around the pile to increase the interface resistance. Prefabricated geotextile tube was wrapped around the steel reinforcement as shown in Fig. 1. The reinforcement was then placed into the predrilled shaft hole. Twelve hours after casting the piles, cement slurry was injected into the geotextile tubes via high pressure (< 2 Mpa) to form the pile helices. The diameter of the piles used in situ was around 600 mm, with a length of around 35 m. The diameter of the

*Corresponding author, Professor, E-mail: qianjiangu@tongji.edu.cn

http://www.techno-press.org/?journal=gae&subpage=7 ISSN: 2005-307X (Print), 2092-6219 (Online)

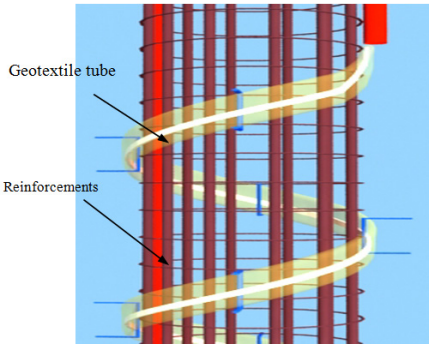

Fig. 1 Geotextile tubes around the reinforcements for later construction of helical piles

ribs was in the range of 120 mm to 200 mm. The rib spacing ranges from 600 mm to 2000 mm. This type of pile has been successfully used in many projects and proved to be cost effective comparing to traditional helical piles and can be used in other part of the world with similar ground conditions (Huang *et al*. 2013). Though helical piles have been successfully used in practice, and the behaviour of the piles has been extensively studied using physical tests or numerical modelling (Abdelghany and El Naggar 2011, Juran and Komornik 2006, Iskander and Hassan 1998, Kurian and Shah 2009, Papadopoulou *et al*. 2014, Mittal and Mukherjee 2015), the design method varies with soil condition, construction method and type of piles used (Guo and Yu 2016).

Many researchers have studied the behaviour of steel or concrete helical piles in various soil conditions using numerical modelling, laboratory and in-situ tests (Livneh and El Naggara 2008, Ghaly *et al*. 1991, Tsuha *et al*. 2012). Using in-situ tests, Abbasov and Kovalevskii (1984) studied flat-corrugated piles in sand and found that the inclusion of the ribs can increase the bearing capacity of the piles by a factor of up to 70%. Research also found that the increase of number of helices does not always increase the capacity of the piles (Clemence *et al*. 1994, Sakr 2009). Lutenneger (2011) observed that, in sand the efficiency of multi-helix anchors can be affected by many factors including the relative helix spacing. Elsherbiny and El Naggar (2013) studied the effect of spacing of helices using 3 dimensional numerical modelling and found that the decrease of helix spacing may reduce the compressive bearing capacity of helical piles.

The interaction between soil and pile is much affected by the interface behaviour, which is a combination effect of soil properties and the structure's surface topography (Potyondy 1961, Coyle and Sulaiman 1967, Kulhaway and Peterson 1979). Dove and Jarrett (2002) summarized that soil and structure interface can be non-dilative or dilative depending on the roughness of the structure interface, and indicated that for surfaces with dilative shearing behaviour, the interface resistance can be as great, or greater, than the soil shear resistance. Using laboratory and numerical modelling, Dove and Jarrett (2002) and Wang *et al*. (2007) studied the effect of surface roughness on the interface shear behaviour by varying the root spacing (the spacing between the roots of the asperities), asperity spacing (the spacing between the peaks of the asperities), asperity height and asperity angle of machined, idealized surface with asperity height in the order of 0 to 0.65 mm (with particle size in the range of 0.5 mm to 0.7 mm). The authors found that, maximum interface efficiency is affected by the asperity spacing to median grain diameter ratio, asperity height to median grain diameter ratio, and asperity angle. To achieve interface efficiency of approximately 1.0, Dove and Jarrett (2002) suggested that the asperity height should be about equal to the median

grain diameter, and the asperity spacing should be one to three times the median grain diameter. The authors also suggested that, 90-degree asperity angel is not required to maximize the interface shear strength. The authors did not observe passive wedge in the soil for a 90 degree ribbed surface, but they suggested that passive zone may occur when asperity height and asperity spacing to particle diameter ratios are high. Irsyam and Hryciw (1991) and Hryciw and Irsyam (1990, 1993) tested the shear behaviours between Ottawa 20-30 sand particles (a uniform, poorly-graded quartz sand produced by the U.S. Silica Company of Ottawa, IL., with D50 around 0.72 mm) and slabs with square (rib height 2.5 mm) and trapezoidal ribs (rib height 0.6 mm). They found that the shear zone thickness is affected by the shape of the ribs. Passive zone can develop ahead of the square ribs but not ahead of the trapezoid ribs, therefore the shear behaviour between the soil and the plates with trapezoid shaped ribs is more affected by the properties of the soil rather than the inclusion of ribs, as soil particles can easily "roll over" the trapezoid ribs. Hossain (2010) compared shear behaviour of soil between slabs with inclusion of channels, geogrid meshes, geosynthetic sheet, expanded metal mesh, square mesh and chicken mesh, and found that inclusion of channels on cement sheet is the most effective in increasing the shear resistance at the interfaces.

Comparing to traditional helical piles and ribbed slabs, the helices of the piles used in Shanghai reported by Qian *et al*. (2013) are relatively small comparing to the diameter of the piles but greater than the height of asperities used in the reported tests discussed earlier, and the shape of the helices is not the regular shape as reported (triangle, rectangular or trapezoidal). The current methods used in practice for helical piles and other ribbed structures cannot be directly used in the design of this type of piles or the analysis of the soil pile interface interaction. The reinforcing mechanism of the ribs and the selection criteria of rib spacing are not clear. Therefore, there is a lack of guideline in the design of such piles, and it is necessary to better understand the interaction between the soil and the ribbed concrete surfaces to propose a proper design method.

Ring shear apparatus (Yoshimi and Kishida 1981), simple shear (Uesugi and Kishida 1986a, b), dual interface testing apparatus (Paikowsky *et al*. 1995) and direct shear test (Hossain and Yin 2014, Gu *et al*. 2003, Zhou *et al*. 2012) have been used to test soil structure interface behaviour and each of the methods has its own advantages and disadvantages. This paper describes a set of large scale direct shear tests on soil and ribbed concrete slabs interface to reveal the reinforcing mechanism of the inclusion of ribs in this type of helical piles used in Shanghai. Three dimensional numerical modelling were carried out with an ABAQUS finite element code to analyse the soil and ribbed concrete interaction. It was found that the inclusion of the ribs affects the failure zones at the interface and increases the pull out resistance of ribbed concreted in sand. The failure mode, the shape and thickness of the shear failure surfaces vary with the spacing of the ribs. The increment of the frictional resistance is affected by the normalized rib spacing, e.g., the ratio of the rib spacing to the rib's diameter. Based on the test and numerical modelling results, it was found that an optimum normalized rib spacing to maximize the frictional resistance may exist for this type of structures.

2. Test program

2.1 Test equipment

The tests were carried out in a large shear box designed and manufactured in Tongji University (SJW-200), China. The dimension of the shear box is 600 mm on the shear direction, 400 mm wide, and 200 mm deep. The load capacity is 200 kN on both vertical and horizontal directions.

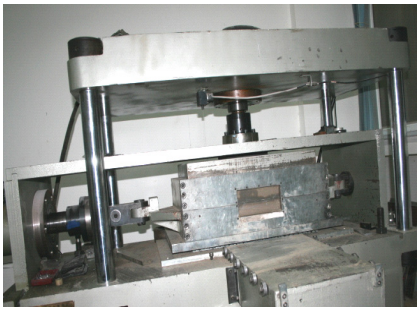

Fig. 2 The large-scale direct shear apparatus (SWJ-200)

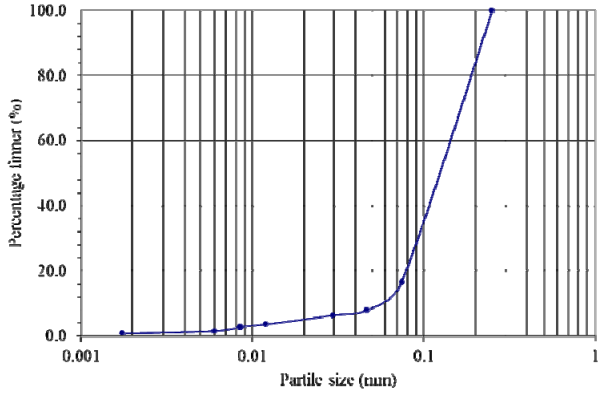

Fig. 3 Particle size distribution of the silty sand used in the tests

The shear rate can be set at 0.1 to 50 mm per minute. The maximum displacement is 50 mm on vertical, and 150 mm on shear direction. The shear box is shown in Fig. 2. The front panels of the shear box are detachable, so that the panels can be removed to observe the soil deformation at the shear interface after the tests.

2.2 Soil and concrete plate

The soil samples were taken from Changxing Island, Shanghai, China. The layer of soil is located 2 m below the ground with a thickness of 16 m. Soil in this layer is normally consolidated silty sand according to the USCS system. Bulk soil samples were collected from the site, broken down, sieved and well mixed with water to a water content of 9.6% (in-situ water content) for test. The particle size distribution of the soil is shown in Fig. 3.

2.3 Concrete slabs

To simulate the rib effect of the cast in-situ helical piles and the reinforcement mechanism, ribbed concrete slabs were used in the laboratory to study the soil and pile interface resistance. The pull-out resistance of helical piles is a complicated three dimensional problem. To study the soil and pile interface behaviour, the three dimension problem was simplified into a plane strain model by considering the circumference of the pile, using “cut and unfold techniques” as shown in Fig.

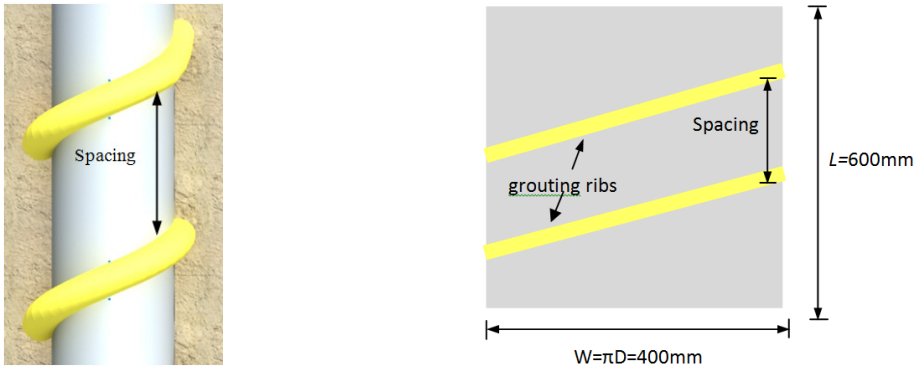

(a) (b)

Fig. 4 Transforming the three dimensional problem (a) into a plane strain problem (b)

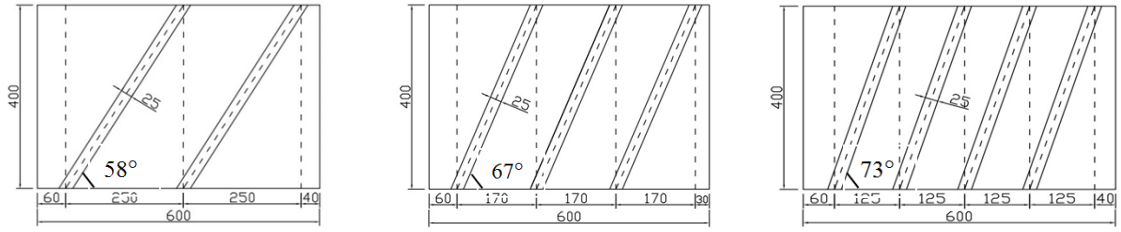

(a) Diagrams of the ribbed concrete

(b) Samples of the ribbed concrete

Fig. 5 Diagram and samples of the ribbed concrete slabs

4(a) shows a ribbed pile, and Fig. 4(b) shows a section of the unfolded pile surface with the width of $w = \pi D$, in which D is the diameter of the pile. For a pile with a diameter of 400 mm, the unfolded width is about 1.3 m, which is too large for the shear box. Therefore, only a section of the unfolded surface is simulated in the large shear box, e.g., 600 mm wide. During the transformation, the inclination of and the distance between the ribs were kept unchanged. Therefore the shear behaviour between the pile and soil interface can be simulated by shearing a ribbed concrete slab in a direct shear box with infill soils.

C30 concrete mixed at the 0.55 water-cement ratio was used to fabricate the ribbed concrete slabs. The dimension of the slab is 600 mm × 400 mm × 50 mm. The ribs are 25 mm in diameter and 12.5 mm in height, which is about 1/6 of the ribs used in situ. The concrete slabs were cured for 28 days under standard conditions for the full development of the strength before testing (Chinese Standard 2003). Concrete slabs with rib spacing of 125 mm (4 ribs), 170 mm (3 ribs) and

250 mm (2 ribs) were manufactured to simulate a 400 mm diameter pile with rib height of 150 mm commonly used in practice. The model to prototype ratio is about 1:6. The angles between the ribs and the shear direction are roughly 73, 67 and 58 degrees respectively. The diagrams and the samples of the concrete slabs with ribs are shown in Fig. 5. As a comparison, a flat concrete slab without ribs was also manufactured to test the shear behaviour of soil and concrete interface in the large shear box.

2.4 Test preparation and procedure

Since the concrete slab is 50 mm in thickness, and the bottom half of the shear box is 100 mm deep, concrete cubes were placed underneath the concrete slabs for levelling to make sure the shear is along the upper surface of the slabs. The slab surfaces were moistened to minimizing absorption of water from soil samples. Soil samples were weighted and placed into the upper box in four layers and slightly compacted to a relative density of 0.51 with unit weight of 15.4 kN/m^3, which is the soil density in-situ. Direct shear tests on the soil samples at this initial density showed that the friction angle of the soil is 34.8 degree and 1 kPa for cohesion. It is to note that the small amount of cohesion observed may be due to the effect of matric suction, as the water content used in the tests was 9.6%. The properties of the soils are shown in Table 1.

After the soil samples were placed in the shear box, a small vertical load (10 kPa) is applied overnight for consolidation. After consolidation, the front panel of the upper box was removed and a series of vertical colour bands were painted on the front surface of the soil using water resistant black paint to monitor the deformation of the soil during shear as shown in Fig. 6. The front panel was then replaced on to the shear box after the paint dries.

Load was applied via hydraulic actuators. Horizontal displacement was monitored using LVDTs. The vertical and horizontal loads and horizontal movement of the shear box were logged at the interval of 0.4 s using automatic data logger system connected to a personal computer. The

Table 1 Properties of the silty sand in natural condition

	Water content (%)	Unit weight (kN/m^3)	Void ratio			Relative density	Cohesion (kPa)	Friction angle (°)
			e	e_{max}	e_{min}			
Property	9.6	15.4	0.92	1.2	0.65	0.51	1	34.8

Fig. 6 Color band at the front surface of the soil

samples were tested under the vertical load of 100 kPa, 150 kPa and 200 kPa at the rate of 2 mm/min to a maximum lateral displacement of 40 mm. The shearing rate is similar to that of a typical displacement-controlled field test in sand, as recommended in Institution of Civil Engineers (2007). At this rate, sand will remain fully drained at the soil-plie interface (Lam *et al*. 2013).

3. Test results

3.1 Shear resistance

The displacement curves of the samples were normalized with the height of the ribs and plotted against shear force in Fig. 7. The figures show that, for different concrete slabs, the shear stress vs. normalized displacement curves follow a similar pattern. Under different vertical loading levels, the shear resistance at the interface stabilizes when the displacement is about twice the rib height. It shows that the inclusion of ribs increased the shear resistance between the soil and concrete slabs. The resistance does not increase consistently with the number of ribs, but peaks when the number of ribs is 3 as shown in Fig. 8. The shear stress and normal stress relationship was plotted in Fig. 9. The results show that, without ribs, the friction between soil and concrete surface is about 34.5° in the large shear box, slightly less than the friction angle of the soil. With 2, 3, and 4 ribs, the friction angles at the shear surfaces are 38.2, 40.7 and 39.8 degrees, which have increased 10%, 17% and 14% respectively. It is to note that for ribbed concrete, the friction angle used herein is not the friction angle between the soil and concrete interface, but an 'equivalent friction angle (δ_r)' to calculate the ratio between the equivalent shear stress (pull out force (F) / flat area of the concrete slab (A)) and the equivalent normal pressure (normal force (P) / flat area of the concrete slab (A))

$$\tan(\delta_r) = \frac{F/A}{P/A} \tag{1}$$

For cases without ribs, the friction angle (δ_r) reflects the friction between the soil and concrete interface. So the equivalent friction angle can be described by introducing an interface dilation angle β as follows

$$\delta_r = \phi + \beta \tag{2}$$

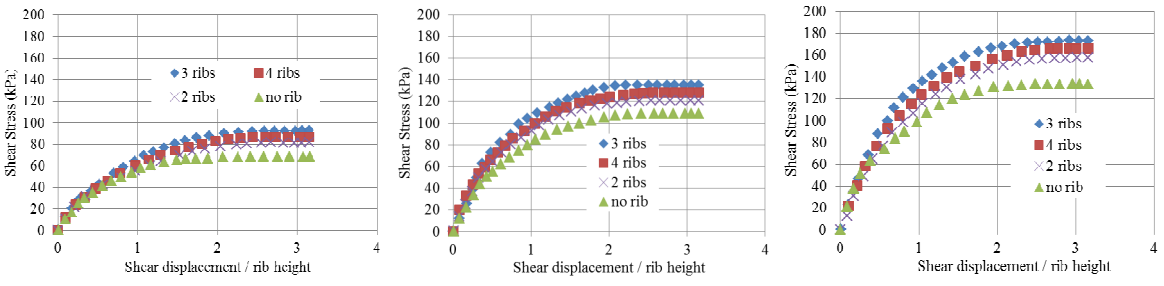

(a) (b) (c)

Fig. 7 Shear force and normalized displacement curves under the vertical load of: (a) 100 kPa; (b) 150 kPa; and (c) 200 kPa

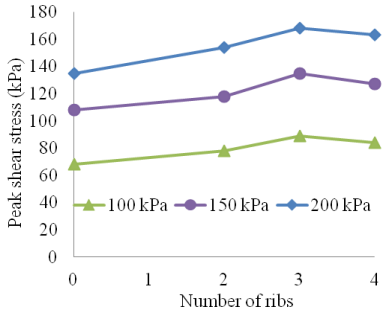

Fig. 8 Peak resistance against number of ribs

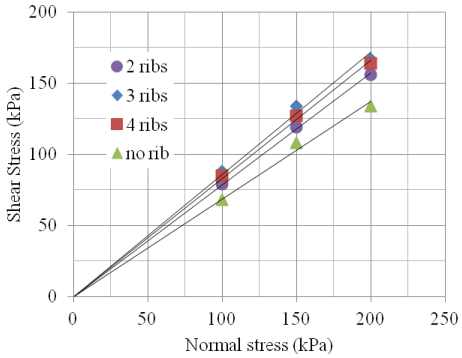

Fig. 9 Shear stress and normal stress relationship of the tested samples

The increase of pull out resistance, or the equivalent friction angle, may be caused by the increase of contact area between soil and concrete slab. But the results show that β does not increase linearly with the number of ribs, but peaks at certain conditions. This indicates that the increase of shear resistance is not purely by the increase of contact area between soil and concrete interface. The mechanism of this phenomenon will be explained in the following sections.

3.2 Deformation at the interface

After finishing the tests, the front panel of the upper box was removed from the shear box. The deformation of the soils at the interface was analyzed by connecting the point of maximum curvature of each vertical columns with curves, as shown in Fig. 10. It can be seen that passive zones (the zones that subjected to passive soil pressure due to the movement of the ribs) have developed ahead of the ribs, which agrees with the finding from Hryciw and Irsyam (1993) on rectangular ribs, and supports the statement by Dove and Jarrett (2002) that significant strength increment can occur at sand and rough surfaces, and passive wedges can form when rib height and rib spacing to particle diameter ratios are large enough. Hryciw and Irsyam (1993) reported that for trapezoidal ribs, no passive zone can be developed. This may be due to the fact that the height of the trapezoidal ribs was only 0.6 mm, whilst the height of the rectangular ribs used in their tests was 2.5 mm. Zhou *et al*. (2012) also observed passive zones ahead of the ribs of geogrids (oval shape ribs with thickness of 5 mm and width of 6.3 mm) during pull out tests in medium sand. This may suggest that as the height of the ribs increases, passive zone may develop ahead of the

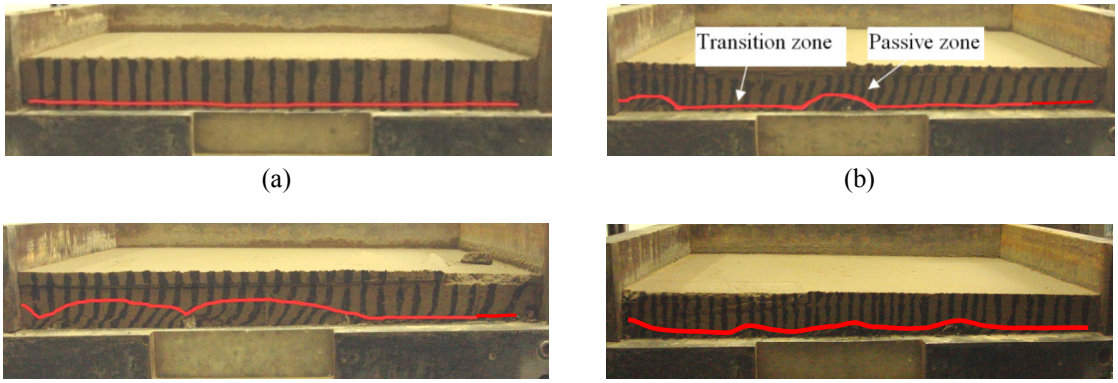

Fig. 10 Shear deformation of soils at the slab and soil interface: (a) smooth concrete; (b) two ribs; (c) three ribs; and (d) four ribs

ribs irrespective of their shapes.

It can be seen that the size and the thickness of the passive zones in the three slabs with ribs are different, and the size of the passive zones is the largest at the interface of the slab with three ribs. As rib spacing getting larger, e.g., 2 ribs, the passive zones are widely separated from each other with a transition zone, and as rib spacing getting smaller, the passive zones are interconnected as shown in Fig. 10(d) for slabs with four ribs, which make the shear zone becomes flatter and the shear behaviour is more affected by the soil properties. The shear surface is very smooth along the interface between the soil and the slab with no rib. The shapes of the shear surface also support the findings by Hryciw and Irsyam (1993), Wang *et al*. (2007), and Wang and Jiang (2011) that the spacing between ribs may affect the development of the passive zones and the thickness of the shear zone.

As suggested by Paikowsky *et al*. (1995), the roughness of failure surface can be categorized into three types: "smooth" for slabs with four ribs, "intermediate" for slabs with two ribs, and "rough" for slabs with three ribs. Based on the shapes of the shear surface and the passive zones described with the red lines shown in Fig. 10, the failure mode of the interface can be classified as: "local shear failure" for "intermediate failure zones" in slabs with 2 ribs (Fig. 10(b)), when the rib spacing is too large and the passive zones are not fully developed and widely separated; "punching shear failure" for slabs with 4 ribs (Fig. 10(d)), when the passive zones are too close and the passive zones are slightly larger than the size of the ribs and the failure zone is relatively "smooth"; and "general shear failure" when the spacing of the ribs is at its optimum value and the passive zones are fully developed (rough) between the ribs. The different failure modes and the roughness of the shear surfaces may explain the higher shear resistance in the slab with three ribs. This will be further discussed in the following sections with numerical modelling.

4. Numerical modelling

The tests were modelled with a Finite Element Model in ABAQUS 6.10. Concrete is modelled with elastic material with Young's modulus E = 30 GPa, Poisson's ratio υ = 0.2. The soil is modelled with Mohr-Coulomb material, with E = 39 MPa, υ = 0.3, friction angle ϕ = 34.8°, unit

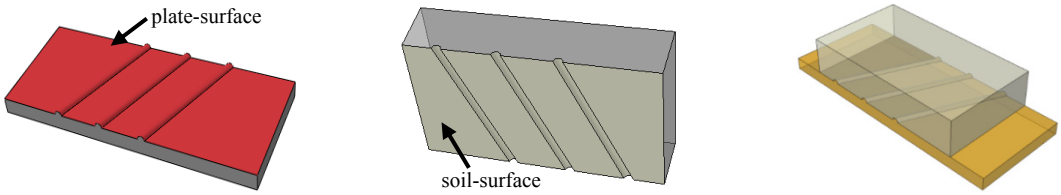

(a) Slab body and surface (b) Soil body and surface (c) Assembled structure

Fig. 11 Concrete slab and soil body parts used in the numerical modelling

(a) Meshes of the concrete slab (b) Meshes of the soil body

Fig. 12 Finite element meshes used in the numerical modelling

weight γ = 15.4 kN/m^3. A dilation angle of 0° is assumed for the loose sand as obtained from laboratory tests, which agrees with the recommendations by Houlsby (1991). A small apparent cohesion c = 1 kPa is assumed for the soil to consider the possible contribution of suction to the soil, and to avoid numerical instability in the model.

The soil body and concrete slabs are modelled with two separate parts. The two parts were assembled via soil surface (in the soil body) and slab surface (in the slab body). A typical soil body and slab body (with 3 ribs) are shown in Fig. 11, and the ones with the meshes shown in Fig. 12.

4.1 Soil and concrete interface modelling

The results of the numerical models can be affected by many factors, e.g., the soil and interface models adopted. There are many models to simulate the behaviour of soil and structure interface, including constitutive modelling, interface elements and contact algorithms (Gomez and Ebeling 1999, Goodman *et al*. 1968, Katona 1983, Kaliakin and Li 1995, Villard 1996, Zienkiewicz *et al*. 1970). The models can be nonlinear elastic (Desai 1985) or elasto-plastic (Gennaro and Frank 2002, Mortara *et al*. 2002, Zeghal and Edil 2002). There are also models developed by using the disturbed-state concept (Desai and Ma 1992), damage mechanics (Hu and Pu 2004) and critical state soil mechanics (Liu *et al*. 2006). Zhou *et al*. (2011) modelled pull out behaviour of soil nailing with Coulomb's friction model using the observed parameters of disturbed soils in the shear zone. Esterhuizen *et al*. (2001) suggested using plasticity models for shear behaviour between soil and geosythetics.

The sensitivity of the interface behaviour to the models is another interesting topic to be further investigated. Since the main purpose of the paper was not to study the constitutive behaviour of the interfaces, one of the most widely used hyperbolic models developed by Duncan and Chang (1970) based on the works by Kondner (1963) and Kondner and Zelasko (1963) was used to model the soil and concrete interface in the three dimensional finite element analysis.

Clough and Duncan (1969, 1971) described the shear stress and displacement curve of the interface using

$$\tau = \frac{w_s}{a + bw_s} \tag{3}$$

in which τ is shear stress on the contact surface, w_s is the relative tangential displacement between soil and concrete slab, a and b are fitted parameters using the shear and displacement curve obtained from shear tests

$$a = \frac{1}{k_{si}}, \qquad b = \frac{1}{\tau_u} \tag{4}$$

In the equation, k_{si} and τ_u are the initial shear stiffness and asymptotic shear stress value obtained from the hyperbolic curve as shown in Fig. 13.

In the model, τ_u is normally larger than the peak shear stress τ_f, therefore, Clough and Duncan (1971) used a failure ratio (R_f) to describe the difference

$$\tau_f = R_f \tau_u \tag{5}$$

The initial stiffness k_{si} is expressed as

$$k_{si} = Kp_a \left(\frac{\sigma_n}{p_a} \right)^n \tag{6}$$

in which σ_n and p_a are normal stresses on the contact surface and atmospheric air pressure respectively, n and K are the dimensionless numbers to be determined from curve fitting method. For sand and concrete interface, we can assume zero cohesion at the interface

$$\tau = \sigma_n \tan\theta \tag{7}$$

where θ is the interface friction angle. By substituting Eqs. (3) to (6) into Eq. (7), we obtain

$$\tau = \frac{w_s}{\dfrac{1}{Kp_a \left(\dfrac{\sigma_n}{p_a} \right)^n} + \dfrac{R_f w_s}{\sigma_n \tan\theta}} \tag{8}$$

By differentiating the above equation with respect to w_s, the tangential stiffness of the interface can be expressed as

$$k_{st} = \frac{\partial \tau}{\partial w_s} = Kp_a \left(\frac{\sigma_n}{p_a} \right)^n \left(1 - \frac{R_f \tau}{\sigma_n \tan\theta} \right)^2 \tag{9}$$

For a 3D model, the tangential shear stiffness includes two orthogonal components, i.e., k_{stx} and k_{sty}. In this analysis, we consider $k_{st} = k_{stx} = k_{sty}$ for simplicity. To obtain the parameters used in the model, the shear displacement curve obtained from the soil and non-ribbed concrete slab was fitted

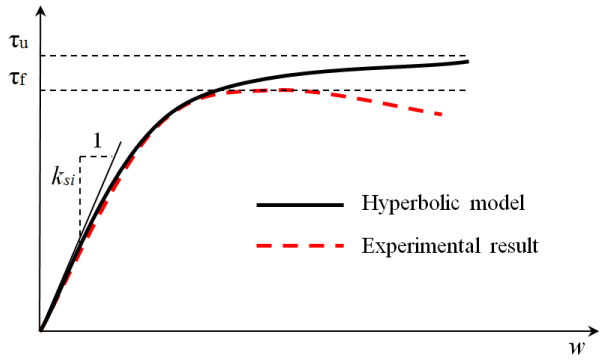

Fig. 13 Clough and Duncan (1971) hyperbolic interface model

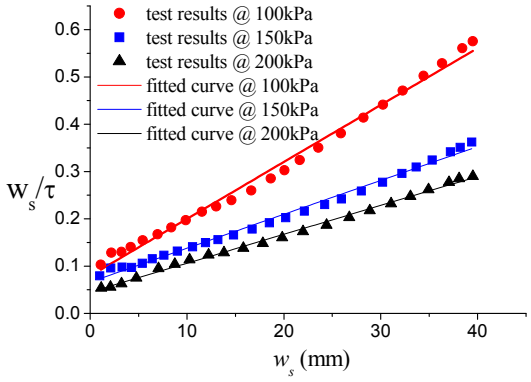

Fig. 14 Shear displacement curve fitting to obtain the parameters for the hyperbolic contact model

Table 2 Parameters used in soil and concrete interface model

σ_n (kPa)	a	b	τ_u (kPa)	τ_f (kPa)	R_f	θ (°)
100	7.94×10^{-5}	0.012	83.3	68.6	0.82	34.5
150	6.62×10^{-5}	0.0072	138. 9	108.6	0.78	35.9
200	4.46×10^{-5}	0.0062	161.3	133.6	0.83	33.7

as shown in Fig. 14. The fitted parameters are shown in Table 2. The mean values of R_f (0.8) and θ (34.7°, which is very close to the measured value) are used to drive K and n, which are 120.448 and 0.807 respectively, and the values were used in the model described in Eq. (9) to simulate the interface stiffness.

4.2 Modelling results

The tested and modelled shear stress vs. displacement curves of the samples without ribs and with three ribs under the loading level of 100 kPa, and the sample with three ribs under the loading level of 150 kPa and 200 kPa are compared in Fig. 15. The comparison shows that the numerical model well captured the shear behaviour of the samples. The differences observed in the

experimental and numerical results, especially at higher stress levels shown in Fig. 15(b) may be due to the simplification of interface behaviour with the hyperbolic model shown in Fig. 13. The variation of the shear stress and shear displacement curves observed in the tests shown in Fig. 14 cannot be fully captured with the linear function. This could be another reason contributes to the differences between the simulated and experimental results in Fig. 15.

The shear surface deformation development of the slab with three ribs during the shear is shown in Fig. 16. It can be seen from the figures that, on shear direction, the influence zone of the ribs increases with the displacement. At lower displacement levels, the shape of the plastic zone around the ribs is similar to that of the slab with 2 ribs as shown in Fig. 10. This is because, at lower strain levels, the deformation around the ribs is mainly affected by the interaction between soil and individual ribs. After 20 mm of displacement, the influence zones started to connect with each other. This results in the peak of the shear resistance after 20-25 mm of displacement as shown in Fig. 7. At failure, e.g., after 20 mm of lateral displacement, the thickness of the passive zone ahead of the ribs can be up to 3 times the height or the radius of the ribs, which is similar to

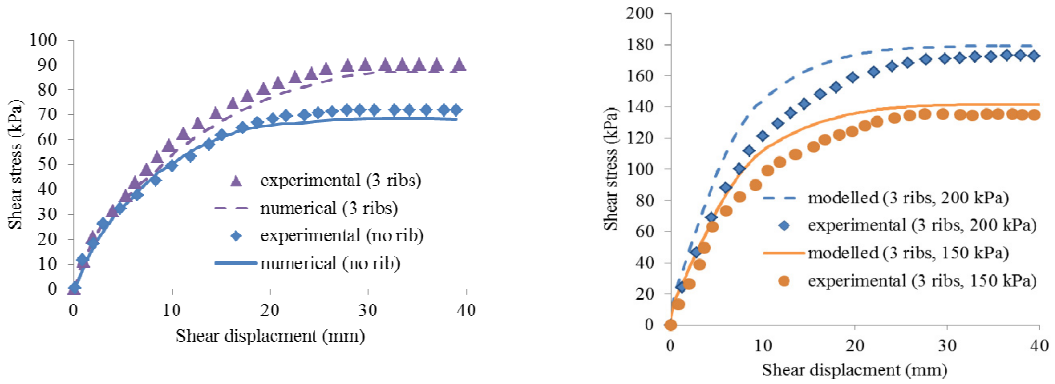

(a) (b)

Fig. 15 The comparison of tested and modelled shear displacement curves of: (a) the samples without ribs and with ribs under the load level of 100 kPa; and (b) the sample with three ribs under the loading of 150 kPa and 200 kPa

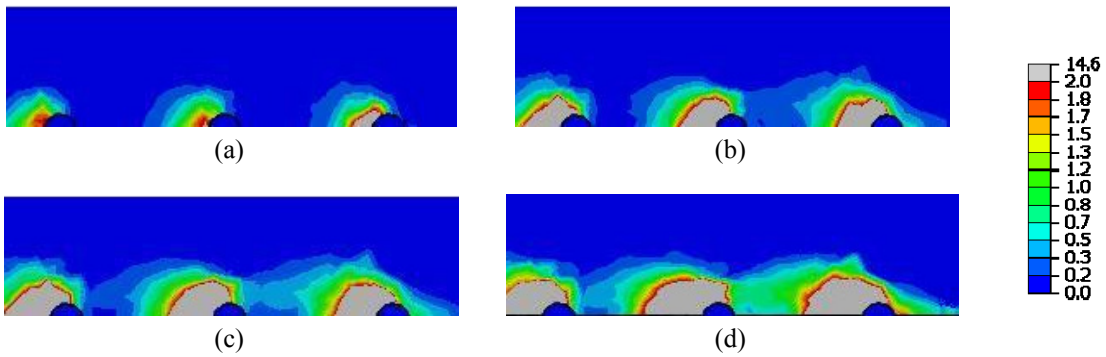

(a) (b)

(c) (d)

Fig. 16 Modeled plastic zones around the ribs at the displacement of: (a) 10 mm; (b) 20 mm; (c) 30 mm; and (d) 40 mm

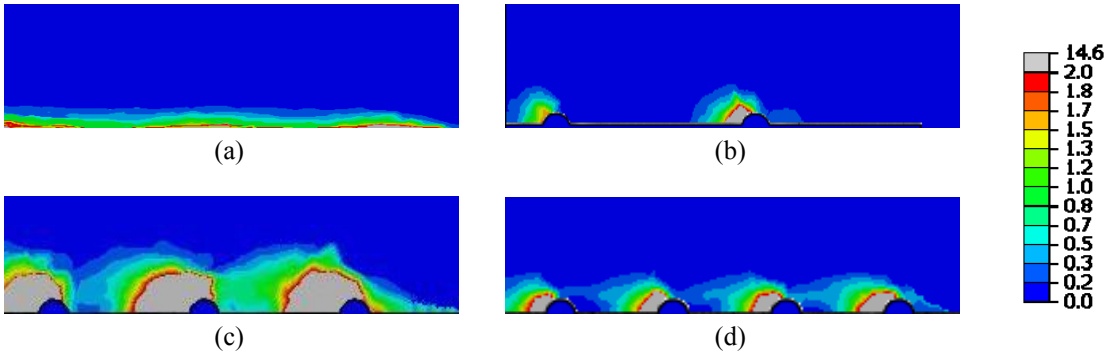

Fig. 17 Modeled shear strain at the interface with: (a) no rib; (b) 2 ribs; (c) 3 ribs; and (d) 4 ribs, at the displacement of 40 mm

the ratio of the influence zone observed by Zhou *et al*. (2012) at the soil and geogrid interface. Fig. 17 shows that at failure, the thickness of the shear zone is the thickest for the slab with three ribs and thinnest for the flat slab. This agrees with the findings from Hryciw and Irsyam (1993) that the thickness of influence zone is affected by the spacing of the ribs, as the spacing of the ribs affects the development of passive zones and the mobilization of soil particles around the ribs. It is to note that, in Fig. 17(a), a thin shear zone has been observed at the soil and smooth concrete interface in the numerical model, which has not been observed in the experimental test as shown in Fig. 10(a). This may due to the mesh size effect used in the numerical model, which may exaggerate the deformation at the interface.

5. Reinforcing mechanism

From Figs. 10 and 17 we can see that, with the inclusion of ribs, "undulated" shear surfaces were created and resulted in profound dilation behaviours at the soil-concrete interface, with respect to the interface without rib. The roughness of the shear surface is the largest at the concrete slab with three ribs, which results in the largest increment of interface friction angle.

To further explain the optimum rib spacing, the influence zone of a single rib is simulated in

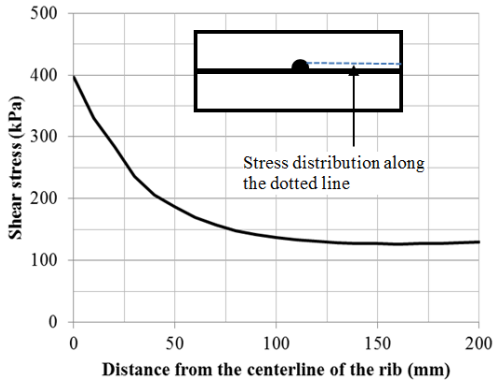

Fig. 18 Shear stress distribution on the surface at the middle height of the rib

ABAQUS by removing the two side ribs from the slab with three ribs. The shear stress variation along the surface at the middle height of the rib is plotted in Fig. 18. The figure shows that the shear stress along this surface is greater near the rib, and reduces with distance from the rib. The influence of the rib on shear stress in the soil body diminishes at the distance of 150 mm from the rib, which is about 6 times of the rib's diameter. This value supports the observed optimum normalized rib spacing described earlier (6.8) if the lateral displacement of the slab is considered (20 mm at failure, which is 80% of the rib's diameter). At smaller normalized rib spacing, e.g., less than 6, overlap of the influence zones may occur, whilst at larger normalized rib spacing, e.g., 10 or greater, the contribution of the ribs to the shear resistance becomes less due to the discontinuity of the passive zones. This explains the overlap of the failure zones observed in the slab with 4 ribs when the normalized rib spacing is 5, and the discontinuity of the failure surfaces in the slab with 2 ribs. Based on the observation, for half cylindrical shape ribs, it is suggested that the optimum spacing between the ribs is about 7 times the diameter of the ribs. This value is much greater than the values (1 to 3) found by Dove and Jerrett (2002) for geomembranes.

6. Conclusions

Cast in-situ grouted helical pile becomes a popular option for uplift piles in Shanghai, China. The piles were cast in situ and cement grout was injected into geotextile tubes pre-wrapped around the steel reinforcements to form the helices. To test the effect of the ribs on the strength increment of the ribbed piles, ribbed concrete slabs with parallel ribs spaced at different angles to the centreline of the slabs were sheared in soil infilled large scale direct shear box. The shear tests were carried out using silty sand and concrete slabs with no, two, three and four ribs. The front panels of the shear box are detachable so that the deformation at the shear surface can be observed using coloured soil bands. The tests were simulated with a 3 dimensional finite element code on ABAQUS. The test and numerical modelling results shows that:

- The inclusion of ribs increased the friction resistance by up to 17%, e.g., the equivalent friction angle at the interface increased from 34.5° (soil and concrete interface) to 40.7° (with three ribs). The interface friction angle does not increase consistently with the spacing of the ribs, but peaks when there are three ribs.
- The deformation of the coloured soil bands reveals that passive zone can develop ahead of the half cylindrical shaped ribs. The length and height of the passive zones are affected by the spacing of the ribs. When rib spacing is too large, the passive zones are separated by transition zones. When rib spacing is too close, the passive zones cannot be fully developed. At optimum spacing, the number of fully developed passive zones is the maximum, which results in the maximum soil interface resistance.
- The roughness of the shear failure surfaces in the soil body can be categorized as "smooth", "intermediate" or "rough" based on the number of fully developed passive zones and the length of the transition zones, which are affected by the spacing of the ribs. The failure mode at the interface can be classified as punching, general or local shear failure depending on the roughness of the failure surfaces. At large rib spacing, the roughness of shear surface is intermediate and it results in a local shear failure. If the spacing is too dense, the failure surface will be smooth and a punching shear failure may occur at the interface. At optimum spacing, passive zones ahead of the ribs are well developed and connected with each other

to form a set of continuous arches therefore the failure surface is rough which will result in a general shear failure. The shear resistance is the highest when general shear failure occurs.

- Numerical modelling on the soil and single ribbed concrete interface indicates that, for half cylindrical ribs, the depth of the passive zone ahead of a single rib is about 6 times of the rib's diameter, which agrees with the test results of slabs with three ribs, with rib spacing and rib height ratio of about 6.8. For the design of ribbed piles, more tests should be done on model piles of different rib spacing to determine the contribution of ribs to the pullout resistance of ribbed piles considering the three dimensional effect of ribs.

In the physical and numerical models, the shear was forced to along the flat surface of the slabs. It is worth to note that if the location of the shear interface changes, e.g., along the top or middle height height of the ribs, the authors would anticipate different results. Further research should be done to investigate the location of the shear surface in such structures and their effect on the shear behaviour at the interface.

Acknowledgments

The project is funded by the Key Program of Shanghai Science and Technology Committee (Grant Nos. 11231202002, 07dz12006).

References

Abbasov, P.A. and Kovalevskii, A.A. (1984), "Behavior of piles with ribbed surfaces in sand soil", *Soil Mech. Found. Eng.*, **21**(2), 69-75.

Abdelghany, Y. and El Naggar, H. (2011), "Steel Fibers Reinforced Grouted and Fiber Reinforced Polymer Helical Screw Piles—A New Dimension for Deep Foundations Seismic Performance", In: *Geo-Frontiers 2011: Advances in Geotechnical Engineering*, (J. Han and D.E. Alzamora Eds.), ASCE, Geotechnical Special Publication No. 211, Reston, VA, USA, pp. 103-112.

Chinese Standard (2003), GB/T 50081-200200; Standard for test method of mechanical properties on ordinary concrete.

Clemence, S.P., Crouch, L.K. and Stephenson, R.W. (1994), "Prediction of uplift capacity for helical anchors in sand", *Proceedings of the 2nd Geotechnical Engineering Conference*, Cairo, Egypt, January, Volume I, pp. 332-343.

Clough, G.W. and Duncan, J.M. (1969), "Finite element analyses of Port Allen and Old River Locks", Army Engineer Waterways Experiment Station, Report No. TE-69-3; Vicksburg, MS, USA.

Clough, G.W. and Duncan, J.M. (1971), "Finite element analyses of retaining wall behaviour", *J. Soil Mech. Found. Div., ASCE*, **97**(SM12), 1657-1673.

Coyle, H.M. and Sulaiman, I. (1967), "Skin friction for steel piles in sand", *J. Soil Mech. Found. Div.*, **93**(6), 261-270.

Desai, C.S. and Ma, Y. (1992), "Modeling of joints and interfaces using the disturbed-state concept", *Int. J. Numer. Anal. Meth. Geomech.*, **16**(9), 623-653.

Desai, C.S. (1985), "Cyclic testing and modeling of interfaces", *J. Geotech. Eng, ASCE*, **111**(GT6), 793-815.

Dove, J.E. and Jarrett, J.B. (2002), "Behavior of dilative sand interfaces in a geotribology framework", *J. Geotech. Geoenviron. Eng.*, **128**(1), 25-37.

Duncan, J.M. and Chang, C.Y. (1970), "Nonlinear analysis of stress and strain in soils", *J. Soil Mech. Found. Div., ASCE*, **96**(SM5), 1629-1653.

Elsherbiny, Z.H. and El Naggar, M.H. (2013), "Axial compressive capacity of helical piles from field tests

and numerical study", *Can. Geotech. J.*, **50**(12), 1191-1203.
Esterhuizen, J.J.B., Filz, G.M. and Duncan, J.M. (2001), "Constitutive behaviour of geosynthetic interfaces", *J. Geotech. Geoenviron. Eng.*, *ASCE*, **127**(10), 834-840.
Gennaro, V.D. and Frank, R. (2002), "Elasto-plastic analysis of the interface behavior between granular media and structure", *Comput. Geotech.*, **29**(7), 547-572.
Ghaly, A., Hanna, A. and Hanna, M. (1991), "Uplift Behavior of Screw Anchors in Sand. I: Dry Sand", *J. Geotech. Engrg.*, **117**(5), 773-793.
Goodman, R.E., Taylor, R.L. and Brekke, T.L. (1968), "Model for mechanics of jointed rock", *J. Soil Mech. Found. Div.*, **94**(SM3), 637-659.
Gomez, J.E. and Ebeling, R.M. (1999), "Development of an Improved Numerical Model for Concrete-to-Soil Interfaces in Soil-Structure Interaction Analyses", US Army Corps of Engineers, Technical Report ITL-99-1.
Gu, X.M., Seidel, J.P. and Haberfield, C.M. (2003), "Direct shear test of sandstone concrete joints", *Int. J. Geomech.*, **3**(1), 21-33.
Guo, Y. and Yu, X.B. (2016), "Design and analyses of open-ended pipe piles in cohesionless soils", *Front. Struct. Civ. Eng.*, **10**(1), 22-29.
Hossain, Md.Z. (2010), "A study on thin cementitious composite (TCC) materials for soil reinforcement applications", *Australian J. Agri. Eng.*, **1**(4), 153-159.
Hossain, M.A. and Yin, J.H. (2014), "Behavior of a pressure-grouted soil-cement interface in direct shear tests", *Int. J. Geomech.*, **14**(1), 101-109.
Houlsby, G.T. (1991), "How the dilatancy of soils affects their behaviour", *Proceedings of the 10th European Conference on Soil Mechanics and Foundation Engineering*, Florence, Italy, May.
Hryciw, R.D. and Irsyam, M. (1990), "Shear zone characterization in sands by carbowax impregnation", *Geotech. Test. J.*, **13**(1), 49-52.
Hryciw, R.D. and Irsyam, M. (1993), "Behavior of sand particles around rigid ribbed inclusions during shear", *Soils Found.*, **33**(3), 1-13.
Hu, L.M. and Pu, J.L. (2004), "Testing and modeling of soil-structure interface", *J. Geotech. Geoenviron. Eng. ASCE*, **130**(8), 851-860.
Huang, M.S., Qian, J.G. and Zhang, C.R. (2013), "Performance and analysis of non-conventional uplift piles in soft ground", *International Symposium on Advances in Foundation Engineering*, Singapore, December.
Institution of Civil Engineers (2007), ICE specification for piling and embedded retaining walls, Thomas Telford, London, UK.
Irsyam, M. and Hryciw, R.D. (1991), "Friction and passive resistance in soil reinforced by plane ribbed inclusions", *Geotechnique*, **41**(4), 485-498.
Iskander, M.G. and Hassan, M. (1998), "State of the practice review: FRP composite piling", *J. Compos. Construct.*, *ASCE*, **2**(3), 116-120.
Juran, I. and Komornik, U. (2006), "Behavior of fiber-reinforced polymer composite piles under vertical loads", U.S. Department of Transportation, Federal Highway Administration, Publication No. FHWA-HRT-04-107.
Kaliakin, V.N. and Li, J. (1995), "Insight into deficiencies associated with commonly used zero-thickness interface elements", *Comput. Geotech.*, **17**(2), 225-252.
Katona, M.G. (1983), "A simple contact friction interface element with applications to buried culverts", *Int. J. Numer. Anal. Meth. Geomech.*, **7**(3), 371-384.
Kondner, R.L. (1963), "Hyperbolic stress-strain response: Cohesive soils", *J. Soil Mech. Found. Div.*, *ASCE*, **89**(SM1), 115-143.
Kondner, R.L. and Zelasko, J.S. (1963), "A hyperbolic stress-strain formulation for sands", *Proceedings of the 2nd Pan-American Conference on Soil Mechanics and Foundations Engineering*, Sao Paulo, Brazil, July, Volume I, pp. 289-324.
Kulhaway, F.H. and Peterson, M.S. (1979), "Behavior of sand and concrete interfaces", *Proceedings of the 6th Pan American Conference on Soil Mechanics and Foundation Engineering*, Sao Paulo, Brazil, July, Volume 2, pp. 225-230.

Kurian, N.P. and Shah, S.J. (2009), "Studies on the behaviour of screw piles by the finite element method", *Can. Geotech. J.*, **46**(6), 627-638.
Martin, C., Jefferis, S. and Lam, C. (2014), "Effects of polymer and bentonite support fluids on concrete–sand interface shear strength", *Geotechnique*, **64**(1), 28-39.
Liu, H.B., Song, E.X. and Ling, I.L. (2006), "Constitutive modeling of soil-structure interface through the concept of critical state soil mechanics", *Mech. Res. Commun.*, **33**(4), 515-531.
Livneh, B. and El Naggara, M.H. (2008), "Axial testing and numerical modeling of square shaft helical piles under compressive and tensile loading", *Can. Geotech. J.*, **45**(8), 1142-1155.
Lutenneger, A.J. (2011), "Behavior of multi-helix screw anchors in sand", *Proceedings of the 14th Pan-American Conference on Soil Mechanics and Geotechnical Engineering*, Toronto, ON, Canada, October.
Mittal, S. and Mukherjee, S. (2015), "Behaviour of group of helical screw anchors under compressive loads", *Geotech. Geol. Eng.*, **33**(3), 575-592.
Mortara, G., Boulon, M. and Ghionna, V.N. (2002), "A 2-D constitutive model for cyclic interface behaviour", *Int. J. Numer. Anal. Meth. Geomech.*, **26**(11), 1071-1096.
Paikowsky, S.G., Player, C.M. and Connors, P.J. (1995), "A dual interface apparatus for testing unrestricted friction of soil along solid surfaces", *Geotech. Test. J.*, **18**(2), 168-193.
Papadopoulou, K., Saroglou, H. and Papadopoulos, V. (2014), "Finite element analyses and experimental investigation of helical micropiles", *Geotech. Geol. Eng.*, **32**(4), 949-963.
Potyondy, J.G. (1961), "Skin friction between various soils and construction material", *Geotechnique*, **11**(4), 339-353.
Qian, J.G., Chen, H.W. and Huang, M.S. (2013), "Numerical modeling pile-soil interface of grouting screw uplift pile", *International Symposium on Advances in Foundation Engineering*, Singapore, December. DOI: 10.3850/978-981-07-4623-0_129
Sakr, M. (2009), "Performance of helical piles in oil sand", *Can. Geotech. J.*, **46**(9), 1046-1061. DOI: 10.1139/T09-044
Tsuha, C.H.C., Aoki, N., Rault, G., Thorel, L. and Garnier, J. (2012), "Evaluation of the efficiencies of helical anchor plates in sand by centrifuge model tests", *Can. Geotech. J.*, **49**(9), 1102-1114.
Uesugi, M. and Kishida, H. (1986a), "Influential factors of between steel and dry sands", *Soils Found.*, **26**(2), 33-46.
Uesugi, M. and Kishida, H. (1986b), "Frictional resistance at yield between dry sand and mild steel", *Soils Founda.*, **26**(4), 139-149.
Villard, P. (1996), "Modelling of interface problems by the finite element method with considerable displacements", *Comput. Geotech.*, **19**(1), 23-45.
Wang, J. and Jiang, M. (2011), "Unified soil behavior of interface shear test and direct shear test under the influence of lower moving boundaries", *Granular Matter*, **13**(5), 631-641.
Wang, J., Dove, J.E. and Gutierrez, M.S. (2007), "Determining particulate–solid interphase strength using shear-induced anisotropy", *Granular Matter*, **9**(3-4), 231-240.
Yoshimi, Y. and Kishida, T. (1981), "A ring torsion apparatus for evaluation friction between soil and metal surface ", *Geotech. Test. J.*, **4**(4), 145-152.
Zeghal, M. and Edil, T. (2002), "Soil structure interaction analysis: modeling the interface", *Can. Geotech. J.*, **39**(3), 620-628.
Zienkiewicz, O.C., Best, B., Dulllage, C. and Stagg, K.G. (1970), "Analysis of nonlinear problems with particular reference to jointed rock systems", *Proceedings of the 2nd International Congress on Society of Rock Mechanics*, Beograd, Serbia, September, Volume 3, pp. 501-509.
Zhou, W.H., Yin, J.H. and Hong, C.Y. (2011), "Finite element modelling of pullout testing on a soil nail in a pullout box under different overburden and grouting pressures", *Can. Geotech. J.*, **48**(4), 557-567.
Zhou, J., Chen, J.F., Xue, J.F. and Wang, J.Q. (2012), "Micro-mechanism of the interaction between sand and geogrid transverse ribs", *Geosynth. Int.*, **19**(6), 426-437.

GC